ChemPubSoc Europe

DOI: 10.1002/cphc.201700300

CHEMPHYSCHEM Articles

Diameter-Sensitive Breakdown of Single-Walled Carbon Nanotubes upon KOH Activation

Jianglin Ye,[a] Shuilin Wu,[a] Kun Ni,[a] Ziqi Tan,[a] Jin Xu,[a] Zhuchen Tao,[a] and Yanwu Zhu*[a, b]

While potassium hydroxide (KOH) activation has been used to create pores in carbon nanotubes (CNTs) for improved energy-storage performance, the KOH activation mechanism of CNTs has been rarely investigated. In this work, the reaction between single-walled CNTs (SWCNTs) and KOH is studied in situ by thermogravimetric analysis coupled to infrared (IR) spectroscopy and gas chromatography/mass spectrometry (MS). The IR and MS results clearly demonstrate the sequential evolution of CO, hydrocarbons, CO_2, and H_2O in the activation process. By using the radial breathing mode of Raman spectroscopy, a diameter-sensitive selectivity is observed in the reaction between SWCNTs and KOH, leading to a preferential distribution of SWCNTs with diameters larger than 1 nm after activation at 900 °C and a preferential removal of SWCNTs with diameters below 1 nm upon activation.

1. Introduction

Single-walled carbon nanotubes (SWCNTs) have attracted much research attention due to their unique physical properties and potential applications in various fields including optoelectronics, field-effect transistors, fuel cells and energy storage.[1–3] Metallic SWCNTs (*m*-SWCNTs) and semiconducting SWCNTs (*s*-SWCNTs) co-exist in the products prepared by commonly-used methods such as arc discharge and chemical vapor deposition.[4–6] Many approaches have been proposed for the separation of *m*-SWCNTs from *s*-SWCNTs or vice versa, for better-defined properties or applications of SWCNTs. Among them, methane plasma hydrocarbonation has shown effective to selectively etch *m*-SWCNTs with *s*-SWCNTs remaining on the growth substrate.[7] Hydrogen plasma has led to a diameter-dependent etching of SWCNTs,[8] in which SWCNTs with diameter of smaller than 1 nm were completely converted to hydrocarbon gas species, as a result of etching by neutral and positive ions of H species in the plasma. In addition, a gas-phase reaction between fluorine and SWCNTs followed by an annealing has been demonstrated for selectively etching *m*-SWCNTs with diameters of less than 1.1 nm.[9] In the reaction, fluorine molecules are strongly chemisorbed during fluorination, and *m*-SWCNTs with small diameters tend to be disintegrated into CF_n gas species during the following thermal treatment. In another work, SO_3 was used to selectively etch *s*-SWCNTs at 400 °C based on the cycloaddition functionalization on *s*-SWCNTs.[10]

Chemical activation, such as KOH activation, is an effective method to develop porosity in carbon materials for improved energy-storage performance.[11,12] A typical activated carbon (AC) obtained from KOH activation of cokes has demonstrated a specific surface area (SSA) of 2700 $m^2 g^{-1}$.[13] By KOH activation of microwave exfoliated graphite oxide (MEGO), a three-dimensional (3D) carbon (called aMEGO) has been obtained showing an SSA of up to 3100 $m^2 g^{-1}$ and simultaneously ≈100% sp^2 carbon bonding, leading to a gravimetric capacitance of up to 200 $F g^{-1}$ and excellent power performances in organic electrolytes.[14] In general, KOH activation for the preparation of ACs includes three stages:[15] 1) etching of carbon by a redox reaction at temperatures above 400 °C based on Equation (1):

$$6\,KOH + C \leftrightarrow 2\,K + 3\,H_2 + 2\,K_2CO_3; \quad (1)$$

2) the decomposition of K_2CO_3 and development of nanopores by H_2O, CO, and CO_2 at temperatures above 700 °C; and 3) K intercalation into graphitic walls, which results in a lattice expansion of the carbon.

In terms of the reaction between KOH and well sp^2-hybridized carbons, such as MEGO, our study showed that holes were created in graphene platelets at relatively low reaction temperatures (e.g. starting from 350 °C) and the following processing at temperatures of higher than 550 °C led to the 3D restructuring of the graphene platelets to the final 3D porous carbon.[16] On the other hand, it was found that the KOH activation at temperatures of 600–800 °C converted C_{60} molecules to a porous 3D carbon with plenty of defects and a high SSA,[17] while carbon quantum dots were obtained when the ratio of KOH to C_{60} is very high (e.g. for KOH:C_{60} = 30:1) in

[a] J. Ye, S. Wu, K. Ni, Z. Tan, J. Xu, Z. Tao, Prof. Y. Zhu
Key Laboratory of Materials for Energy Conversion
Chinese Academy of Sciences and
Department of Materials Science and Engineering
University of Science and Technology of China
Hefei, Anhui 230026 (P.R. China)

[b] Prof. Y. Zhu
iChEM (Collaborative Innovation Center of Chemistry for Energy Materials)
University of Science and Technology of China
Hefei, Anhui 230026 (P.R. China)
E-mail: zhuyanwu@ustc.edu.cn

Supporting Information for this article can be found under: https://doi.org/10.1002/cphc.201700300.

a quick activation (e.g. for a processing of 6≈8 min).[18] Multi-walled carbon nanotubes (MWCNTs) and carbon fibers have also been activated by KOH for improved supercapacitor performances.[19,20] Although the KOH activation of SWCNTs has been explored to increase specific surface area, the mechanisms for the KOH activation of CNTs remain unclear.[21,22] Compare to MWCNTs, the nature properties of SWCNTs probably play a role in the activation process.

In this regard, we address the solid–liquid reaction between SWCNTs and melted KOH by in situ thermogravimetric analysis coupled to infrared spectrometry and gas chromatography/mass spectrometric analysis (TG-IR-GC/MS) in this work. Following the redox reaction, CO is formed and released firstly, and hydrocarbon species formed at around 800 °C, then the more significant evolution of CO_2 and H_2O at temperatures above 825 °C are identified during the following activation procedure. In addition, with resonant Raman spectroscopy it is found that the activation has aroused a preferential etching of SWCNTs with small diameters. The diameter-sensitive reaction of between KOH and SWCNTs could be potentially used to purify SWCNTs and to select SWCNTs with certain diameters and properties.

2. Results and Discussion

In situ thermogravimetric analysis coupled to infrared spectroscopy and gas chromatography mass-spectrometric characterization (TG-IR-GC/MS) was used to trace the reaction between SWCNTs and KOH; the results are shown in Figures 1 a–d. Figure 1 a shows the FTIR spectra measured from the mixture at various temperatures. As we can see, prominent IR bands appear when the heating temperature reaches about 800 °C. Above 800 °C, IR bands at around 670, 1100, 1280, 2050–2250, 2350 and 2700–3100 cm^{-1} dominate the spectra till 925 °C, which is the highest temperature applied in the measurement. Among the bands, those at 670 and 2350 cm^{-1} are typical feature of C=O stretching, suggesting the evolution of CO_2. Moreover, from the spectra we see that the evolution of CO_2 starts at around 825 °C and reaches the maximum at around 875 °C, while the other peaks remain increasing with the temperature. The relatively weak bands at around 1100 and 1280 cm^{-1} are the feature of C-O stretching. Another band in the range of 2050–2250 cm^{-1} is the stretching of CO, which can be clearly identified at 700 °C, by enlarging the corresponding IR spectra in Figure 1 b. Covalent C-H_x groups are

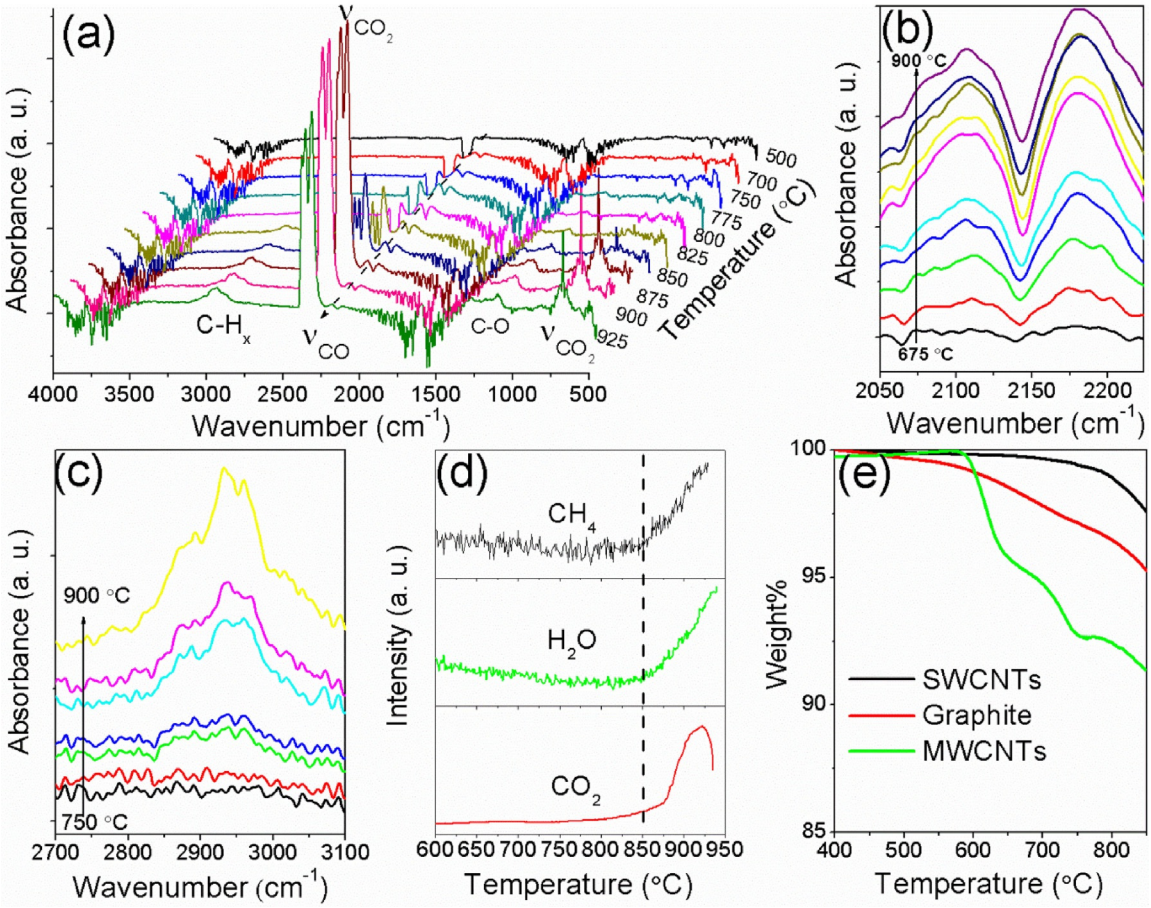

Figure 1. a) FTIR spectra of a SWCNTs/KOH mixture at various heating temperatures measured by in situ TG-IR-GC/MS. b) Enlarged FTIR spectra in the range of 2050–2250 cm^{-1} (corresponding to the CO vibration) from 675 to 900 °C with an interval of 25 °C. c) Enlarged FTIR spectra in the range of 2700 to 3100 cm^{-1} (corresponding to C-H_x vibrations) from 750 to 900 °C with an interval of 25 °C. d) GC-MS analysis showing the evolution of hydrocarbons (CH_4), H_2O, and CO_2 from the SWCNTs/KOH mixture with the temperature. e) TGA curves for a SWCNTs/KOH mixture, together with those of MWCNTs/KOH and graphite/KOH mixtures as references.

visible at 800 °C, as shown in the enlarged IR spectra in Figure 1c, and the intensity is increased with the temperature.[23] The GC/MS results shown in Figure 1d and Figure S1 are generally consistent with the IR spectra, while the slightly different starting temperature in the GC/MS curves could be attributed to the different detection limitation of the GC/MS facility to the gas species. Furthermore, H_2O was detected at the temperature of 850 °C. The TGA results shown in Figure 1e have confirmed the weight loss starting at around 700 °C and a more significant loss at about 800 °C for the mixture of SWCNTs and KOH. In addition, the TG-IR-GC/MS analysis has also been used to trace the reaction between graphite and KOH (Figure S2). The sequential evolution of CO_2 (≈550 °C) and CO (≈700 °C) can be identified. However, no hydrocarbons and H_2O signal can be detected from FTIR spectra and GC-MS analysis. In contrast to SWCNTs, graphite and MWCNTs show a much lower thermal stability in melted KOH as a result of the intercalation of K. Potassium metal atoms produced by reduction reaction can intercalate into graphitic walls so expanding the lattice, the structure can expand further by progressive heating. Specifically, several remarkable weight losses starting from 600 °C were observed from the mixture of MWCNTs and KOH, which is consistent with the lower activation temperature of MWCNTs reported in literatures.[12]

From the in situ TG-IR-GC/MS results, we can identify the sequential evolution of CO (≈700 °C), hydrocarbons (≈800 °C), CO_2 (≈825–850 °C), and H_2O (≈850 °C) gas species from the mixture of SWCNTs and KOH as the temperature increases. Such a reaction between SWCNTs and KOH is different from the previous results on KOH activation of resin, anthracite or MWCNTs, in which the evolution of CO and CO_2 was observed when temperature is higher than 700 °C.[15,12,24] Comparing with the TG-IR-GC/MS results of SWCNTs/KOH, graphite/KOH mixture and previous results, it could be deduced that the mechanism of KOH activation is sensitive to the nature properties of the carbon material. According to the global reaction (1), carbon etching gives rise to the formation of H_2 and K_2CO_3,[24] which may explain the slight weight loss at ≈650 °C due to the release of H_2. At about 700 °C, the following reactions could happen, leading to the generation of CO [Eqs. (2)–(4)]:

$$C(O) \rightarrow CO \quad (2)$$

$$K_2CO_{3+}C \leftrightarrow K_2O + 2\,CO \quad (3)$$

$$K_2O + C \leftrightarrow 2\,K + CO \quad (4)$$

where C(O) is an oxygen surface complex. It is worth noting that the chemisorbed oxygen atoms on the carbon surface of hydroxide or carbonate can gasify carbon atoms to produce CO, thus generating porosity at high temperatures.[15] At the same time, the surface hydrogen complexes (C(H)) developed by adsorption of hydrogen on carbon (C + H→C(H)) could further etch the carbon by sequential gasification to form hydrocarbons at high temperatures (≥800 °C).[25] On the other hand, alkali metal carbonates decompose at temperatures below their melting points in the presence of carbon,[26] which may cause the significant amount of evolution of CO_2 at higher temperatures especially above 850 °C by the Equation (5). The observation of H_2O may be related to the reaction between KOH and CO_2, as shown by Equation (6):

$$K_2CO_3 \leftrightarrow K_2O + CO_2 \quad (5)$$

$$2\,KOH + CO_2 \leftrightarrow K_2CO_3 + H_2O(g) \quad (6)$$

It should be noted that the formation of hydrocarbons has also been reported in the physical activation of Saran char in a steam with the presence of pure hydrogen at ≈850 °C and in phosphoric acid activation of wood containing aliphatic chains at temperatures of lower than 650 °C,[15,27] but rarely reported in chemical activation with KOH. The C(H) complexes formed on SWCNTs surfaces as a result of the chemisorption of hydrogen species might be unstable due to the high curvature and strain of SWCNTs, leading to a high reactivity of SWNTs towards hydrocarbonation (similar to oxidation and hydrogenation in SWCNTs).[8,28] Specifically, the adsorption of H atoms is a sequential procedure, which may result in the formation of C-H_x (x = 1, 2, 3), and of the eventual product CH_4.[29]

Scanning electron microscopy (SEM) images and transmission electron microscopy (TEM) images of SWCNTs before and after being treated with KOH at 800 °C (named as a-SWCNTs-800) and 900 °C (named as a-SWCNTs-900) are shown in Figure 2. From Figure 2a, bundles are observed from original SWCNTs, carbon walls can be observed from the TEM image in Figure 2b. Interestingly, a-SWCNTs remain entangled and the tubular morphology is preserved after being treated with KOH at high temperatures, as seen from Figures 2b,c. Different from the KOH activation of other nanocarbon materials (e.g. microwave expanded graphite oxide and C_{60} molecules),[14] no obvious restructuring has been observed in SWCNTs under the similar KOH treatment conditions. By comparing the TEM images shown in Figures 2d–f, the single-walled hollow structure and large aspect ratio of SWCNTs are reserved after reaction. A close observation has found that the wall became rough, which may be caused by defects. The production yield of SWCNTs after KOH treatment is about 70% at 800 °C and 45% at 900 °C, respectively, suggesting that a significant amount of SWCNTs have been removed by the reaction. The Raman spectra in Figures 2g–i show that the spectra of a-SWCNTs are very similar to that of the original SWCNTs, all with strong G band and weak D band, and the RBM bands.

Figure 3a shows the XPS survey spectra for the original and KOH-processed SWCNTs performed at 600, 700, 800, and 900 °C. A prominent C 1s peak and a noticeable O 1s peak are detected from all samples, without any other significant amount of impurities. Compared to the original SWCNTs, no obvious change can be found in annealed SWCNTs at 800 and 900 °C without KOH (Figure S3). However, there is a significant decrease of the C/O ratio to 7.3 in a-SWCNTs-900. Such oxygen-containing groups can be removed by annealing a-SWCNTs-900 at 900 °C again in argon atmosphere (leading to the sample named as a-SWCNTs-900h, with a C/O ratio of 24.6). The C 1s XPS spectra in Figure 3b show that the C 1s peak for all samples mainly consists of two components, corre-

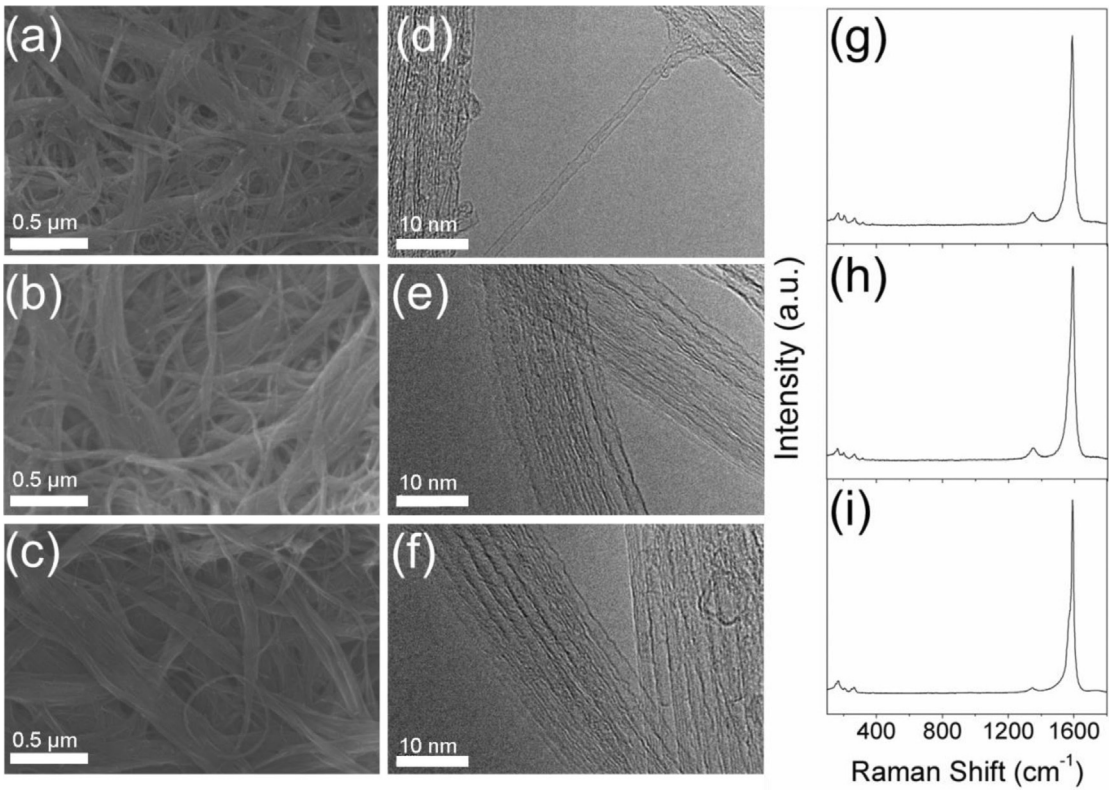

Figure 2. SEM, TEM images and Raman spectra of original SWCNTs (a,d,g) and those treated with KOH at: b,e,h) 800 °C and c,f),i) 900 °C.

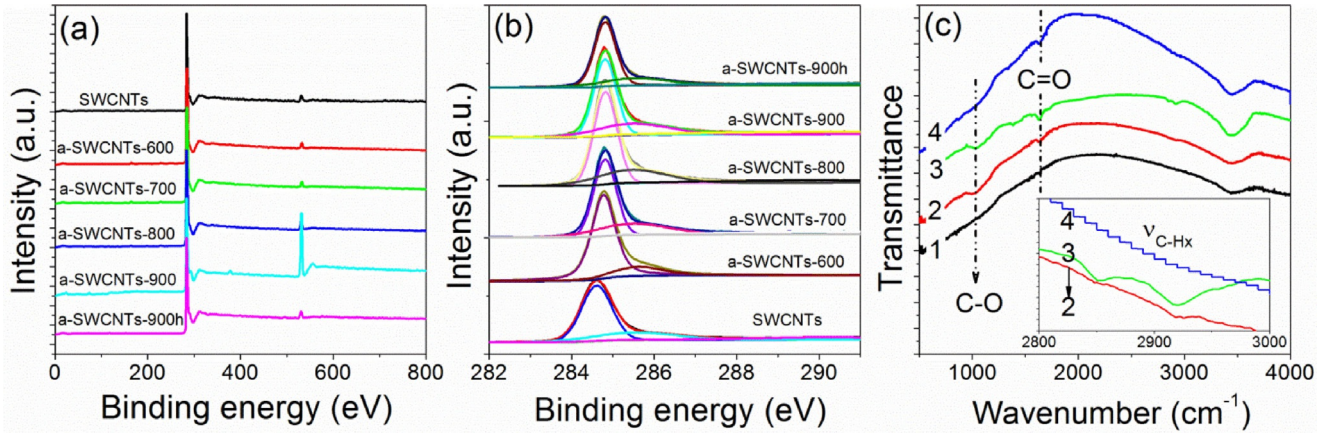

Figure 3. a) XPS survey spectra and b) XPS C 1s spectra of the original SWCNTs and a-SWCNTs obtained at 600, 700, 800, and 900 °C. c) FTIR spectra of the original SWCNTs and a-SWCNTs. Spectrum 1: SWCNTs; Spectrum 2: a-SWCNTs-800, Spectrum 3: a-SWCNTs-900; Spectrum 4: a-SWCNTs-900 h. The inset shows the enlarged spectra in the range of 2800 to 3000 cm^{-1}.

sponding to peaks at 284.6 eV (sp^2 carbon bonding) and 285.5 eV (sp^3 carbon bonding), respectively.[30] The sp^3/sp^2 ratio, which was estimated by integrating the area under the sp^3 or sp^2 peaks, is 0.34, 0.36, 0.39, 0.42, 0.51 and 0.39 for SWCNTs, a-SWCNTs-600, -700, -800, -900 and -900h, respectively. The higher sp^3/sp^2 ratios of a-SWCNTs could come from the covalent bonding of oxygen and hydrogen on the carbon wall, accompanying a shift of the C 1s peak to higher binding energy in a-SWCNTs.[31] The deconvoluted O 1s and K 2p region are shown in Figure S4. The O 1s spectra for all samples mainly consists of two components with C=O (531.2 eV) and C-O (532.7 eV).[32,33] The content of oxygen-containing groups especially C-O increases with the temperature. However, with the rapid desorption of chemisorbed oxygen when the heating temperature reaches about 800 °C, the percentage of C-O decreases, indicating the low stability of C-O. Figure 3c shows the FTIR spectra. The band at 1630 cm^{-1} is ascribed to C=O stretching and that at 1050 cm^{-1} designated as C-O, confirming the presence of a low content yet obvious carbonyl group in both a-SWCNTs-800 and a-SWCNTs-900.[34,35] A close looking

into the range of 2800–3000 cm^{-1} indicates there are bands centered at 2850 and 2920 cm^{-1} (inset of Figure 3c), which can be assigned to the symmetric stretching of sp^3 CH_2, and asymmetric stretching of sp^3 CH_2 or sp^3 CH stretching, respectively. Comparing to that of a-SWCNTs-800, the spectrum of a-SWCNTs-900 shows a stronger vibration in this range, suggesting more C-H_x bonds in a-SWCNTs-900.[8,23] However, C-O and C-H_x stretching are almost eliminated by the second annealing, as shown in the curve of a-SWCNTs-900h, indicating that the stability of C-O and C-H_x groups is low, especially when compared to the C=O group. The observation is consistent with the IR analysis in in situ experiment in terms of the evolution of CO and hydrocarbons formed by desorption of chemisorbed oxygen and hydrogen atoms on carbon.

N_2 adsorption/desorption has been carried out to further investigate the change in the pore structure of SWCNTs upon KOH processing. The isotherms are shown in Figure 4a. It can be seen that the isotherms of original and activated SWCNTs all have a type H4 hysteresis, which is indicative of a silt pore geometry. The BET specific surface area (SSA) of the original SWCNTs is 463.7 m^2g^{-1}. After reaction with KOH at 800 °C and 900 °C, the SSA has been enhanced to 623.6 m^2g^{-1} and 810.5 m^2g^{-1} for a-SWCNTs-800 and a-SWCNTs-900, respectively. The pore size distribution is plotted in Figure 4b by applying a slit pore geometry on micropores and a cylindrical pore geometry on mesopores. The total pore volume has been increased to 0.78 and 1.17 cm^3g^{-1} for a-SWCNTs-800 and a-SWCNTs-900 from 0.58 cm^3g^{-1} for original SWCNTs. A broad pore size distribution in the mesopores range is found for all samples. In contrast, the peak of micropores has shifted to a smaller size after KOH activation, leading to a significant development of pores with size smaller than 1 nm by the KOH processing. A higher activation temperature, for example, 900 °C, has resulted in a higher volume of micropores, with ultra-small pores with size of less than ≈0.7 nm detected from a-SWCNTs-900 till the cutoff at 0.5 nm due to the instrument limitation of N_2 adsorption. Obviously, the activation especially at high temperatures favors the development of micropores in SWCNTs. The formation of CO, hydrocarbons and other oxidization of carbon may have created defects on the wall of SWCNTs or opened the end of SWCNTs, leading to the development of micropores and increase in SSA. It is worth noting that the increase in the volume of micropores and larger SSA in a-SWCNTs have not changed the tubular structure as observed in SEM and TEM. To show the possible effect of enhanced porosity by KOH processing, the supercapacitor performance for a-SWCNTs-900 was compared with the original SWCNTs, as shown in Figure 4c. It shows a much better rate capability with 81% retention at 40 Ag^{-1} (relative to the capacity at 1 Ag^{-1}), due to the fast accessibility of the ions (Fig-

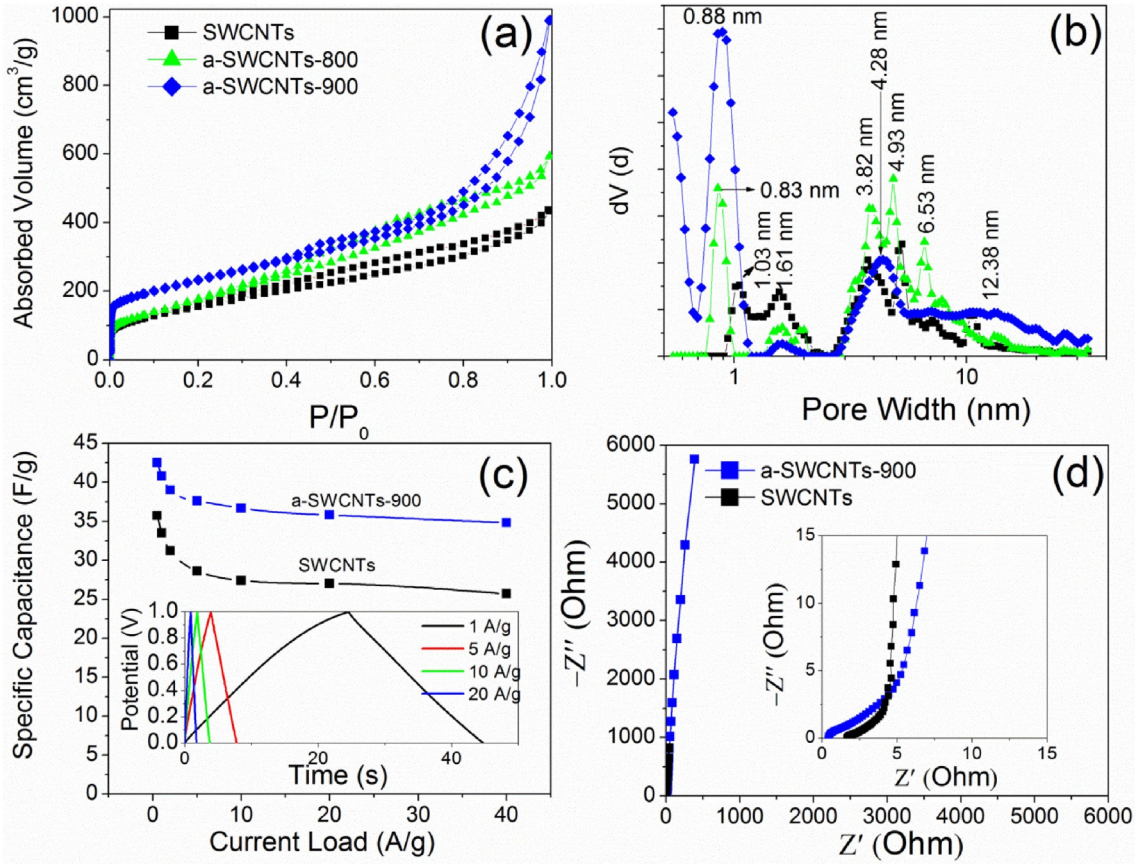

Figure 4. a) N_2 adsorption/desorption isotherms performed at 77 K. b) Pore size distribution of original SWCNTs and a-SWCNTs. c) Supercapacitor performance of a-SWCNTs-900 in 6 M KOH electrolyte. The inset shows the galvanostatic charge–discharge curves of a-SWCNTs-900. d) Nyquist plots of SWCNTs and a-SWCNTs-900.

ure S5). However, the specific capacitance at 1 A g^{-1} has only been increased from 33.5 F g^{-1} for original SWCNTS to 41.2 F g^{-1} for a-SWCNTs-900. Probably because of smaller pores, the charge transfer resistance is large in a-SWCNTs-900, as shown in the Nyquist plots (Figure 4d).

The Raman spectra measured with a laser excitation wavelength of 514 nm clearly show the presence of both *s*- and *m*-SWCNTs with features of the radial breathing mode RBM in the original SWCNTs (Figure 5a).[36] After KOH treatment, those peaks corresponding to higher Raman shifts are largely suppressed and especially for the sample obtained by the second KOH treatment of a-SWCNTs-900 under the same condition (named as a-SWCNTs-900 s), as seen from Figures 5b,c. Specifically, the *m*-SWCNTs with Raman shift at 248 and 266 cm^{-1} were greatly suppressed after reaction with KOH and nearly disappeared after the second KOH treatment. Figures 5d–f show the detailed analysis of the deconvoluted G-bands. For metallic SWNTs, the G-band can be fitted to include a high-frequency Lorentzian component and a low-frequency component with BWF line shape.[37] In addition, a value of $-1/q$ can be obtained from the fitting, which is a measure of the interaction between a continuum of states and phonons, is 0.24 for SWCNTs, further indicating the metallic feature. For a-SWCNTs-900 s, however, the $-1/q$ value is very small ($-1/q = 0.07$), indicating that a-SWCNTs-900 s mainly shows a semiconducting feature.[37] The D-band near 1350 cm^{-1} has not been significantly changed after KOH treatment at high temperatures. The Raman results indicate that SWCNTs reserve the graphitic structure after activation, which is consistent with electron microscopy images. By normalizing the intensities of the Lorentzian peaks obtained in Figure 5a to 5c, the fraction of each peak has been calculated and shown in Figure 5g, with the corresponding diameters shown as the *x*-axis (by using the formula: $\omega_{RBM} = 234/d_t + 10$, d_t is the diameter).[38] As we can see from Figure 5g, the ratio of *s*-SWCNTs with large diameters near 152 cm^{-1} (1.65 nm), 165 cm^{-1} (1.51 nm), and 185 cm^{-1} (1.34 nm) contributes to 39.8% of the original SWCNTs. After KOH treatment, the ratio reaches 55.1% for a-SWCNTs-900 and 68.1% for a-SWCNTs-900s, while the ratio of *m*-SWCNTs with small diameters corresponding to shifts near 248 cm^{-1} (0.98 nm) and 266 cm^{-1} (0.91 nm) is reduced from 28.4% (SWCNTs) to 23.2% (a-SWCNTs-900) and 11.4% (a-SWCNTs-900s). In addition, *s*-SWCNTs with the diameter of 0.78 nm was removed completely. From Figure 5g, it seems that the diameter-dependent selection occurs at about 1.0 nm for the reaction between SWCNTs and KOH at 900 °C.

It is well known that the Raman resonance of SWCNTs is sensitive to the excitation energy of the laser used.[39] Thus, Raman spectra excited by a laser with an excitation wavelength of 785 nm was also performed on the original and KOH-processed SWCNTs and the results are shown in Figures 6a–c. The RBM peaks at 203, 212, 236, 253, 264, and 304 cm^{-1} correspond to *s*-SWCNTs with diameters of 1.21, 1.16, 1.03, 0.97, 0.92, and 0.80 nm, respectively. From the compari-

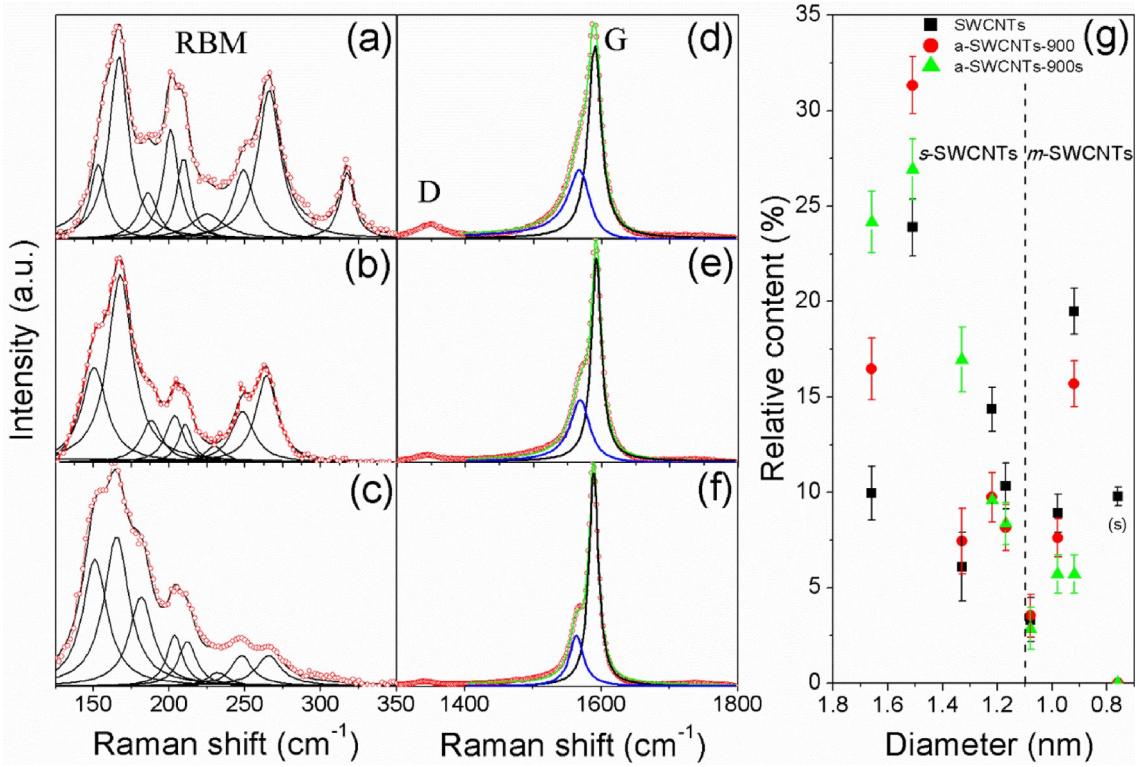

Figure 5. Raman spectra measured with a laser excitation wavelength of 514 nm. Lorentzian deconvolution of RBM modes of: a) SWCNTs, b) a-SWCNTs-900, and c) a-SWCNTs-900 s. d–f) The corresponding fittings of G mode with semiconducting Lorentzian shape and metallic BWF line shape. g) Estimated fractions of SWCNTs, a-SWCNTs-900, and a-SWCNTs-900s with dependence on the diameter. The relative fraction of SWCNTs on each diameter was calculated by normalizing the relative intensities of corresponding Lorentzian peaks.

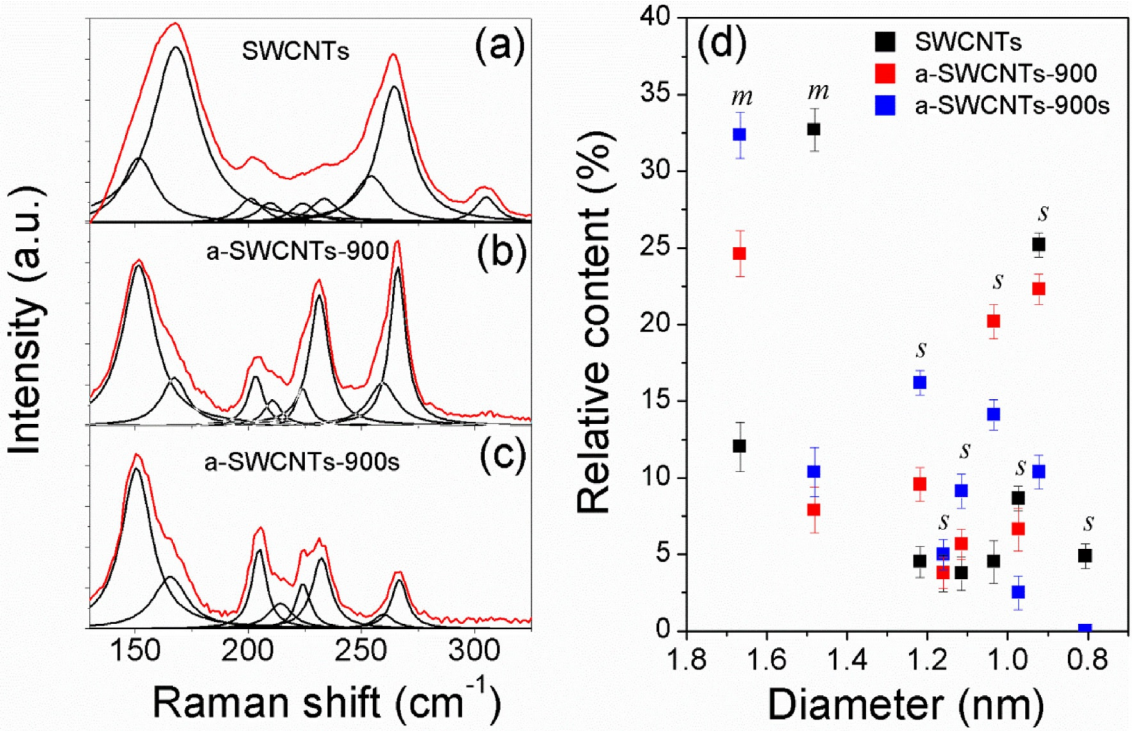

Figure 6. RBM spectra obtained using a laser with an excitation wavelength of 785 nm. *s* and *m* in (d) indicate semiconducting or metallic SWCNTs, respectively.

son shown in Figure 6d, we can see that the *s*-SWCNTs with diameters of less than 1 nm, for example, 0.97 nm, 0.92 nm, and 0.80 nm were suppressed prominently by the KOH reaction. At the same time, a considerable amount of *s*-SWCNTs with diameters ranging from 1.0 to 1.21 nm were maintained, leading to the relatively higher fractions of such *s*-SWCNTs after KOH processing. For *m*-SWCNTs, that with the diameter of 1.48 nm (168 cm^{-1}) was largely removed, leading to a much lower fraction in the activated samples, while that with a diameter of 1.67 nm (150 cm^{-1}) was preserved. The Raman results suggest the selectivity of KOH activation is less sensitive to the diameter for *m*-SWCNTs as a result of the higher chemical reactivity due to more abundant delocalized electronic states in *m*-SWCNTs compared to *s*-SWCNTs.[28] Relative to larger SWCNTs, SWCNTs with smaller diameters have higher radius of curvature and higher strain in the C–C bonding configuration, making them preferentially etched, as also observed in other chemical gas reactions.[7,40] From the Raman results, the relative content of SWCNTs with diameter larger than 1.0 nm in a-SWCNTs-900 s is 89.6% (for 514 nm laser wavelength) or 88.2% (for 785 nm laser wavelength), both remarkably higher than in original SWCNTs (61.2% for 514 nm laser wavelength and 61.4% for 785 nm laser wavelength). Further increase the processing temperatures, for example, to 950 °C, has further improved the selection efficiency based on diameters. The relative content of a-SWCNTs-950 with diameter larger than 1.2 nm ($\omega_{RBM} <$ 205 cm^{-1}) is 75.1% (for SWCNTs: 54.2%), and it's 80.6% from the Raman results with an excitation wavelength of 785 nm (for SWCNTs: 49.2%).

3. Conclusions

In summary, we have investigated the reaction process between SWCNTs and KOH with in situ IR and MS. The chemical activation process starts with redox reaction, and then the sequential evolution of CO, hydrocarbons, CO_2, and H_2O. Among them, oxygen and hydrogen surface complex developed by chemisorption is sequentially gasified to form CO and hydrocarbons, creating nanopores in SWCNT walls and further etching the carbon. With Raman spectra, a diameter-sensitive selectivity is observed. SWCNTs with diameters of less than 1.0 nm are greatly suppressed, while the SWCNTs with diameters greater than 1.6 nm remain unchanged in the radial breathing mode of Raman spectra after activation at 900 °C.

Experimental Section

Materials Processing

The single-walled carbon nanotubes (SWCNTs, 90% purity, 1–3 μm in length) were obtained from Chengdu Organic Chemicals Co., Ltd. To pretreat the CNTs, the as-purchased SWCNTs (500 mg) were first refluxed in 6 M HCl solution at 70 °C for 12 h to remove impurities, and then filtered and washed with deionized water for several times. For in situ thermogravimetric analysis coupled to infrared spectrometry and gas chromatography/mass spectrometric analysis (TG-IR-GC/MS) and thermogravimetric analysis (TGA), 50 mg pretreated SWCNTs were mixed with 250 mg KOH dissolved in ethanol (1 mg mL^{-1}), and then dried at 80 °C under N_2 atmosphere by continuous stirring. Mixtures of graphite/KOH or MWCNTs/KOH were prepared by the same procedures for TGA only. To prepare activat-

ed SWCNTs samples for other characterizations, 120 mg pretreated SWCNTs powder was dispersed in 120 mL ethanol and tip-sonicated for 2 h to obtain a SWCNT suspension. Then, 1.2 g dry KOH was added into the suspension followed by another 2 h of tip sonication for the full dissolution of KOH. The mixture (with a KOH/SWCNTs ratio of 10:1, the higher ratio can make more full reaction between SWCNTs and KOH) was dried by continuous stirring at 80 °C in ambience and loaded into a corundum boat for annealing at 800–900 °C with a heating rate of 5 °C min^{-1} in argon atmosphere. After reaction, the samples were sequentially washed by 1 M HCl, deionized water, and ethanol, and further dried at 60 °C in ambience. The activated SWCNTs are thus named as a-SWCNTs-t, in which t is the reaction temperature.

Characterizations

TGA was carried out using a Q50000 IR (TA instruments, US) in nitrogen in a temperature range of from room temperature to 850 °C with a step of 10 °C min^{-1}. TG-IR-GC/MS was conducted with a TL-9000 system (PerkinElmer, US) in nitrogen atmosphere. Scanning electron microscopy (SEM) images were taken with a JSM-6700F (JEOL, Japan). Transmission electron microscopy (TEM) images were taken with a JEOL-2100F (JEOL, Japan). Nitrogen adsorption was performed by using an automatic adsorption analyzer (Quantachrome Autosorb-iQ, US) at 77 K. The specific surface area of samples was calculated by the Brunauer-Emmett-Teller (BET) equation. Raman spectra were measured using a Labram-HR (Jobin Yvon, France) with a laser excitation at 514 nm and using an inVia Raman microscope (Renishaw, UK) with a laser excitation at 785 nm. X-ray photoemission spectroscopy (XPS) experiment was carried out on a Thermo ESCALAB 250 (Thermo Scientific, US) with $Al_{K\alpha}$ radiation ($h\nu = 1486.6$ eV). Fourier transform infrared spectroscopy (FTIR) spectrum was measured using a Nicolet 8700 (Thermo Scientific, US). Electrochemical measurement was performed on PARSTAT MC (Princeton Applied Research, US).

Acknowledgements

This work was supported by the China Government 1000 Plan Talent Program, China MOE NCET Program, Natural Science Foundation of China (51322204), the Fundamental Research Funds for the Central Universities (WK2060140014 and WK2060140017), and funding from Hefei National Synchrotron Radiation Lab.

Conflict of interest

The authors declare no conflict of interest.

Keywords: activation · diameter · Infrared spectroscopy · radial breathing mode · Raman spectra

[1] J. Opatkiewicz, M. C. LeMieux, Z. Bao, *ACS Nano* **2010**, *4*, 2975 – 2978.
[2] A. Javey, H. Kim, M. Brink, Q. Wang, A. Ural, J. Guo, P. McIntyre, P. McEuen, M. Lundstrom, H. Dai, *Nat. Mater.* **2002**, *1*, 241 – 246.
[3] D. Yu, K. Goh, H. Wang, L. Wei, W. Jiang, Q. Zhang, L. Dai, Y. Chen, *Nat. Nanotechnol.* **2014**, *9*, 555 – 562.
[4] M. Dresselhaus, G. Dresselhaus, R. Saito, *Carbon* **1995**, *33*, 883 – 891.
[5] A. M. Cassell, J. A. Raymakers, J. Kong, H. Dai, *J. Phys. Chem. B* **1999**, *103*, 6484 – 6492.
[6] J. Ding, Z. Li, J. Lefebvre, F. Cheng, G. Dubey, S. Zou, P. Finnie, A. Hrdina, L. Scoles, G. P. Lopinski, *Nanoscale* **2014**, *6*, 2328 – 2339.
[7] G. Zhang, P. Qi, X. Wang, Y. Lu, X. Li, R. Tu, S. Bangsaruntip, D. Mann, L. Zhang, H. Dai, *Science* **2006**, *314*, 974 – 977.
[8] G. Zhang, P. Qi, X. Wang, Y. Lu, D. Mann, X. Li, H. Dai, *J. Am. Chem. Soc.* **2006**, *128*, 6026 – 6027.
[9] C.-M. Yang, K. H. An, J. S. Park, K. A. Park, S. C. Lim, S.-H. Cho, Y. S. Lee, W. Park, C. Y. Park, Y. H. Lee, *Phys. Rev. B* **2006**, *73*, 075419.
[10] H. Zhang, Y. Liu, L. Cao, D. Wei, Y. Wang, H. Kajiura, Y. Li, K. Noda, G. Luo, L. Wang, *Adv. Mater.* **2009**, *21*, 813 – 816.
[11] V. Barranco, M. Lillo-Rodenas, A. Linares-Solano, A. Oya, F. Pico, J. Ibañez, F. Agullo-Rueda, J. M. Amarilla, J. Rojo, *J. Phys. Chem. C* **2010**, *114*, 10302 – 10307.
[12] E. Raymundo-Piñero, P. Azaïs, T. Cacciaguerra, D. Cazorla-Amorós, A. Linares-Solano, F. Béguin, *Carbon* **2005**, *43*, 786 – 795.
[13] H. Marsh, D. S. Yan, T. M. O'Grady, A. Wennerberg, *Carbon* **1984**, *22*, 603 – 611.
[14] Y. Zhu, S. Murali, M. D. Stoller, K. Ganesh, W. Cai, P. J. Ferreira, A. Pirkle, R. M. Wallace, K. A. Cychosz, M. Thommes, *Science* **2011**, *332*, 1537 – 1541.
[15] H. Marsh, F. R. Reinoso, *Activated carbon*, Elsevier, Amsterdam, **2006**.
[16] S. Wu, G. Chen, N. Y. Kim, K. Ni, W. Zeng, Y. Zhao, Z. Tao, H. Ji, Z. Lee, Y. Zhu, *Small* **2016**, *12*, 2376 – 2384.
[17] Z. Tan, K. Ni, G. Chen, W. Zeng, Z. Tao, M. Ikram, Q. Zhang, H. Wang, L. Sun, X. Zhu, *Adv. Mater.* **2016**, *29*, 1603414.
[18] G. Chen, S. Wu, L. Hui, Y. Zhao, J. Ye, Z. Tan, W. Zeng, Z. Tao, L. Yang, Y. Zhu, *Sci. Rep.* **2016**, *6*, 19028.
[19] S.-H. Yoon, S. Lim, Y. Song, Y. Ota, W. Qiao, A. Tanaka, I. Mochida, *Carbon* **2004**, *42*, 1723 – 1729.
[20] E. Frackowiak, S. Delpeux, K. Jurewicz, K. Szostak, D. Cazorla-Amoros, F. Beguin, *Chem. Phys. Lett.* **2002**, *361*, 35 – 41.
[21] L. Ji, Y. Shao, Z. Xu, S. Zheng, D. Zhu, *Environ. Sci. Technol.* **2010**, *44*, 6429 – 6436.
[22] S. M. Lee, S.-H. Park, S. C. Lee, H. J. Kim, *Chem. Phys. Lett.* **2006**, *432*, 518 – 522.
[23] T. Heitz, B. Drevillon, C. Godet, J. Bouree, *Phys. Rev. B* **1998**, *58*, 13957.
[24] M. Lillo-Ródenas, D. Cazorla-Amorós, A. Linares-Solano, *Carbon* **2003**, *41*, 267 – 275.
[25] M. Lussier, Z. Zhang, D. J. Miller, *Carbon* **1998**, *36*, 1361 – 1369.
[26] F. Kapteijn, G. Abbel, J. A. Moulijn, *Fuel* **1984**, *63*, 1036 – 1042.
[27] M. Jagtoyen, F. Derbyshire, *Carbon* **1998**, *36*, 1085 – 1097.
[28] W. Zhou, Y. Ooi, R. A. A. Russo, P. Papanek, D. Luzzi, J. Fischer, M. Bronikowski, P. Willis, R. Smalley, *Chem. Phys. Lett.* **2001**, *350*, 6 – 14.
[29] Z. Zhang, M. G. Lussier, D. J. Miller, *Carbon* **2000**, *38*, 1289 – 1296.
[30] C. Tang, W. Guo, C. Chen, *J. Appl. Phys.* **2010**, *108*, 026108.
[31] T. Okpalugo, P. Papakonstantinou, H. Murphy, J. McLaughlin, N. Brown, *Carbon* **2005**, *43*, 153 – 161.
[32] M. Pumera, H. Iwai, Y. Miyahara, *ChemPhysChem* **2009**, *10*, 1770 – 1773.
[33] A. Ambrosi, M. Pumera, *ChemPhysChem* **2015**, *16*, 331 – 334.
[34] J. Chen, M. A. Hamon, H. Hu, Y. Chen, A. M. Rao, P. C. Eklund, R. C. Haddon, *Science* **1998**, *282*, 95 – 98.
[35] Y. Xu, X. Wang, R. Tian, S. Li, L. Wan, M. Li, H. You, Q. Li, S. Wang, *Appl. Surf. Sci.* **2008**, *254*, 2431 – 2435.
[36] C. Domingo, M. C. García-Gutiérrez, *ChemPhysChem* **2014**, *15*, 4001 – 4005.
[37] S. Brown, A. Jorio, P. Corio, M. Dresselhaus, G. Dresselhaus, R. Saito, K. Kneipp, *Phys. Rev. B* **2001**, *63*, 155414.
[38] M. Milnera, J. Kürti, M. Hulman, H. Kuzmany, *Phys. Rev. Lett.* **2000**, *84*, 1324.
[39] R. Saito, M. Fujita, G. Dresselhaus, U. M. Dresselhaus, *Appl. Phys. Lett.* **1992**, *60*, 2204 – 2206.
[40] Y. Li, S. Peng, D. Mann, J. Cao, R. Tu, K. Cho, H. Dai, *J. Phys. Chem. B* **2005**, *109*, 6968 – 6971.

Manuscript received: March 21, 2017
Revised manuscript received: May 2, 2017
Accepted manuscript online: May 5, 2017
Version of record online: June 1, 2017